Letter Vol. 46, No. 19 / 1 October 2021 / Optics Letters 4797

Optics Letters

Mid-infrared ChG-on-MgF_2 waveguide gas sensor based on wavelength modulation spectroscopy

Mingquan Pi,[1] Chuantao Zheng,[1,*] Huan Zhao,[1] Zihang Peng,[1] Jiaming Lang,[1] Jialin Ji,[1] Lei Liang,[2] Yu Zhang,[1] Yiding Wang,[1] and Frank K. Tittel[3]

[1]State Key Laboratory on Integrated Optoelectronics, College of Electronic Science and Engineering, Jilin University, Changchun 130012, China
[2]State Key Laboratory of Luminescence and Applications, Changchun Institute of Optics Fine Mechanics and Physics, Chinese Academy of Sciences, Changchun 130033, China
[3]Department of Electrical and Computer Engineering, Rice University, Houston, Texas 77005, USA
*Corresponding author: zhengchuantao@jlu.edu.cn

Received 13 August 2021; revised 28 August 2021; accepted 2 September 2021; posted 3 September 2021 (Doc. ID 440361); published 23 September 2021

A novel, to the best of our knowledge, mid-infrared chalcogenide (ChG) on magnesium fluoride (MgF_2) waveguide gas sensor was fabricated by using the lift-off method. MgF_2 was used as a lower cladding layer to increase the external confinement factor for enhancing light–gas interaction. Wavelength modulation spectroscopy (WMS) was used in carbon dioxide (CO_2) detection at the wavelength of 4319 nm (2315.2 cm^{-1}). The limit of detection for the 1-cm-long sensing waveguide based on WMS is ∼0.3%, which is >8 times lower than the same sensor using direct absorption spectroscopy (DAS). The combination of WMS with the waveguide gas sensor provides a new measurement scheme for the performance improvement of on-chip gas detection.

https://doi.org/10.1364/OL.440361

An optical waveguide sensor with small size and high integration [1] can realize the same or similar sensing function as a discrete sensor system with bulk size [2,3]. Direct absorption spectroscopy (DAS) and wavelength modulation spectroscopy (WMS) are two typical techniques used for gas sensing [4]. The principle of WMS is modulating the laser wavelength using a high-frequency sinusoidal signal while scanning the laser wavelength using a low-frequency triangular wave signal. The second harmonic ($2f$) signal, whose amplitude is proportional to the gas concentration, is extracted from the absorption signal. Compared to DAS, the WMS technique is capable of noise suppression (e.g., $1/f$ noise) by using coherent demodulation for sensitivity improvement [4]. However, until now, there is no report of an optical waveguide gas sensor based on WMS, and the reported sensors are generally based on DAS. In 2018, Ranacher *et al*. proposed a silicon (Si) on silicon nitride (Si_3N_4) suspended waveguide carbon dioxide (CO_2 sensor based on DAS with a limit of detection (LoD) of 0.5% [5]. In 2020, Ottonello-Briano *et al*. proposed a suspended silicon-on-insulator (SOI) waveguide CO_2 sensor based on DAS with a LoD of 0.1% [6].

In addition to the spectroscopy technique, the selection of waveguide material is one method to improve sensing performance. The transparent window of magnesium fluoride (MgF_2 can reach 7 μm, which covers the fundamental mid-infrared (MIR) absorption band of most gas species. Also, MgF_2 with a low refractive index of 1.34 at 4319 nm (2315.2 cm^{-1}) [7] is a preferred lower cladding material for decreasing the light power confined in the lower cladding layer. Chalcogenide (ChG) glass with a high refractive index (>2) is transparent in the MIR range. Selecting ChG glass as the waveguide core layer material can decrease absorption loss.

In this Letter, to improve the sensing performance, we proposed a ChG-on-MgF_2 waveguide gas sensor based on WMS. MgF_2 was used as the lower cladding layer to decrease the light power confined in the lower cladding layer. CO_2 was used as the gas analyte with absorption at ∼4319 nm. A CO_2 sensing experiment was performed to verify the feasibility and function of combining the waveguide gas sensor with WMS. A gas sensing experiment based on DAS was also conducted to show the advantage of WMS for noise suppression.

For a waveguide using gas analyte as a cladding layer ($\mathrm{Re}(n_{\mathrm{clad}}) \approx 1$), the external confinement factor (γ), which indicates the interaction effect between light and the gas analyte, can be expressed as [8]

$$\gamma = \frac{n_g \iint_{\mathrm{analyte}} \varepsilon(x,y)|E(x,y)|^2 \mathrm{d}x\mathrm{d}y}{\iint_{\mathrm{total}} \varepsilon(x,y)|E(x,y)|^2 \mathrm{d}x\mathrm{d}y}, \quad (1)$$

where n_g is the group index ($n_g = N_{\mathrm{eff}} - \lambda \mathrm{d}N_{\mathrm{eff}}/\mathrm{d}\lambda$, λ is the wavelength and N_{eff} is the effective refractive index), E is the electric field, and ε is the real part of the permittivity of each layer over the waveguide cross-section. γ is related to (1) the modal gain determined by n_g and (2) the spatial confinement of the energy density to the active sensing region exposed to the target gas [8]. The reported largest γ achieved by a suspended waveguide can be up to 107% [9].

For a MIR waveguide CO_2 sensor system, the emitting beam from the laser first passes through free-space and then enters a MIR fiber for mode coupling with the waveguide. The output

0146-9592/21/194797-04 Journal © 2021 Optica Publishing Group

Corrected 8 October 2021

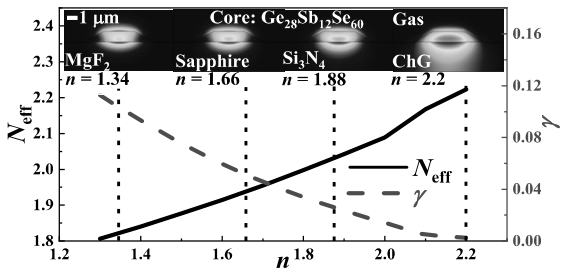

Fig. 1. Curves of N_{eff} (black) and γ (red) of the waveguide versus the lower cladding refractive index n at 4319 nm. Insets: The quasi-TM_0 mode optical field distribution of the waveguide with four typical MIR lower cladding layer transparent materials.

beam from the waveguide will also pass through free-space and is finally focused on a detector. Based on the Lambert–Beer law [10], the light intensity I received by the detector is

$$I = I_0 \exp\left(-\gamma \alpha_{\text{gas}} C_{\text{cell}} L_{\text{s,WG}}\right). \quad (2)$$

Here, $L_{\text{s,WG}}$ is the sensing waveguide length, and C_{cell} is the gas concentration in the cell; α_{gas} is the absorption coefficient; and I_0 is the light intensity received by the detector when $C_{\text{cell}} = 0$, expressed as

$$I_0 = I_{\text{laser}} \exp(-\alpha_{\text{int}} L_{\text{t,WG}} - \alpha_{\text{coupling}}) \exp(-\alpha_{\text{gas}} C_{\text{space}} L_{\text{space}}). \quad (3)$$

Here, $L_{\text{t,WG}}$ is the total waveguide length; α_{coupling} is the coupling loss; α_{int} is the waveguide intrinsic loss, including the material absorption loss and scattering loss and excludes the loss from gas absorption; I_{laser} is the output light intensity from the laser; C_{space} is the CO_2 concentration in free-space; and L_{space} is the free-space length.

A high absorbance $[-\ln(I/I_0)]$ is needed to improve the sensing performance. Curves of N_{eff} and γ of the waveguide versus the refractive index (n) of the lower cladding layer are shown in Fig. 1, where the top width ($Ge_{28}Sb_{12}Se_{60}$, $n = 2.62$) of the core layer is 2.8 μm, the bottom width of the core layer is 6.4 μm, the core layer thickness is 1 μm, and the wavelength is 4319 nm. The quasi-TM_0 mode optical field distribution with four typical MIR lower cladding layer transparent materials [MgF_2 sapphire, Si_3N_4, and ChG glass (Ge-As-S)] are shown in the insets of Fig. 1. N_{eff} increases and γ decreases as n gets larger. The increased N_{eff} indicates that more light power is confined in the dielectric material with a high refractive index. γ is dropped by >40 times when n rises from 1.3 to 2.2. Therefore, using MgF_2 as the lower cladding layer can decrease the light power confined in the lower cladding layer.

The fabrication process is given as follows. First, a MgF_2 layer was deposited on a Si substrate by thermal evaporation (IT-302, LJUHV). Then a $Ge_{28}Sb_{12}Se_{60}$ core layer was fabricated by using the lift-off method. A detailed fabrication process of the lift-off method can be seen in our previous work [11]. Polydimethylsiloxane (PDMS) and a curing agent were mixed at a mass ratio of 10:1 and poured into the 3D-printed mold. The mixture was cured at room temperature to form the PDMS gas cell. Finally, the gas cell with an inlet and an outlet was bonded on the substrate [Fig. 2(b)] by epoxy resin adhesive.

An interband cascade laser (ICL) was used for gas measurement, which mainly emitted polarized light in the vertical direction. So the quasi-TM mode of the waveguide was only considered. The quasi-TM_0 mode optical field distribution of

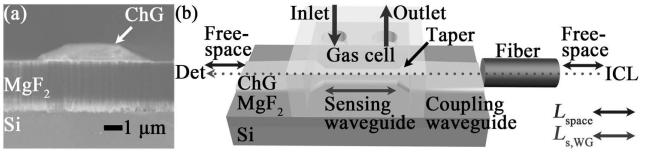

Fig. 2. (a) Scanning electron microscope (SEM) image of the ChG-on-MgF_2 waveguide cross-section structure. (b) Schematic diagram of the waveguide integrated with a PDMS gas cell. Det, detector.

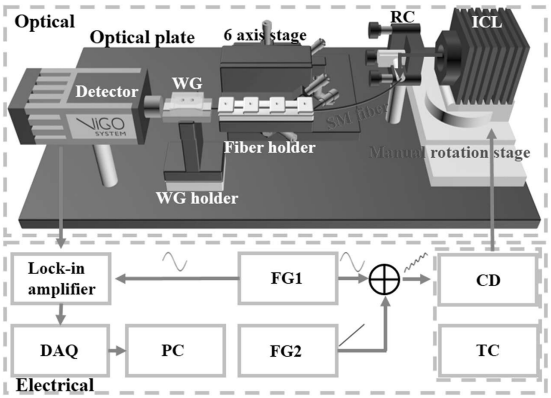

Fig. 3. Schematic diagram of the waveguide gas sensor system based on WMS. CD, current driver; TC, temperature controller; RC, reflective collimator; FG, function generator; PC, personal computer; WG, waveguide; DAQ, data acquisition; SM fiber, single-mode fiber.

the ChG-on-MgF_2 waveguide is shown in the inset of Fig. 1. The γ of the quasi-TM_0 mode waveguide was calculated to be 10.4% based on Eq. (1). Two coupling waveguides on both sides of the sensing waveguide were used for mode coupling. The sensing waveguide length ($L_{\text{s,WG1}}$) is 1 cm, and the width of the coupling waveguide is 16 μm. The main purpose of enlarging the coupling waveguide width is to improve the mode confinement effect of the core layer and to reduce the absorption loss of PDMS [12].

A schematic diagram of the waveguide gas sensor system based on WMS is shown in Fig. 3. The ICL (Nanoplus) was driven by a current driver (LDC210C, Thorlabs) and a temperature controller (TED200C, Thorlabs). A reflective collimator (RC08, Thorlabs), whose reflective lens has a focal length of 33 mm, was used to couple the light into a single-mode indium fluoride (InF_3) fiber (Le Verre Fluoré, France) with a core diameter of 7.5 μm. The waveguide was butt-coupled with the fiber and aligned by a microscope. The output light from the waveguide was directly detected by a Mercury Cadmium Telluride (MCT) detector (PVI-4TE-5, VIGO System). A data acquisition (DAQ) card (USB6211, National Instruments) was used to obtain the data from the lock-in amplifier (SR830, Stanford). A laptop was connected to the DAQ card, and a LabVIEW platform was used to process the data.

The temperature of the ICL was set to 0°C. The scan current range was 31.5–58.5 mA (the wavelength range 4317.28–4321.40 nm) to cover the CO_2 absorption line. The scan signal frequency was 10 Hz, and the modulation frequency was 5 kHz. The absorption of atmospheric CO_2 mainly came from the coupling optical path between the laser and the fiber ($L_{\text{space}} = \sim 7$ cm). We defined a differential $2f$ signal ($D_{2f} = 2f$ signal (C_{cell}) $- 2f$ signal ($C_{\text{cell}} = 0\%$)) to remove

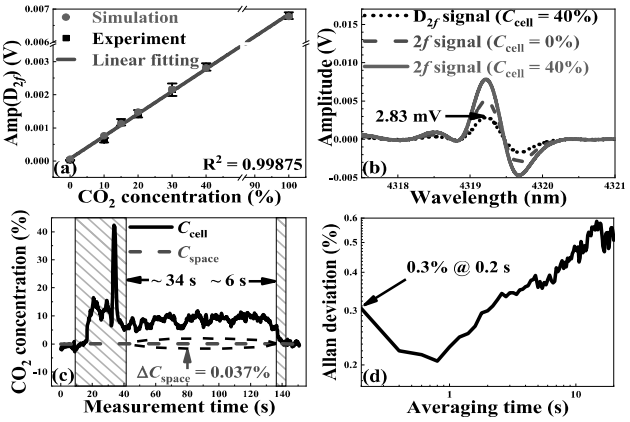

Fig. 4. (a) Simulated and experimental data dots as well as the linear fitting curve of Amp(D_{2f}) versus CO_2 concentration. R^2, goodness of fit. (b) The measured 2f signals for 40% CO_2 (solid) and N_2 (dash) and the differential 2f signal (dot). (c) Dynamic response curve (black) by passing 10% CO_2 into the gas cell followed by a N_2 injection. Curve of the corresponding CO_2 concentration in free-space versus measurement time (red) obtained by the dynamic response curve (black). (d) Allan deviation curve of the sensor.

the background absorption ($C_{cell} = 0\%$). The D_{2f} signal amplitude reached the maximum when the modulation amplitude was optimized as 0.055 V (the corresponding current of 1.02 mA). Since the modulation frequency of the ICL current was as low as 5 kHz, the modulation depth was directly obtained according to the practically measured relationship between the ICL wavenumber and the driving current at an operation temperature of 0°C. The modulation depth is 0.57 times of the full width at the half maximum (0.15 cm^{-1}) of the selected CO_2 absorption line [13]. The experimental D_{2f} signal amplitude within the concentration range of 0–100%, the linear fitting line, and the simulation results are shown in Fig. 4(a). The linear fitting equation between C_{cell} (in %) and the D_{2f} amplitude (Amp(D_{2f}), in V) is

$$C_{cell} = 1.47620 \times 10^4 \,\mathrm{Amp}\left(D_{2f}\right) - 1.00802. \quad (4)$$

The process of the ICL wavelength modulation, the scan of the CO_2 absorption line profile, and the 2f signal extraction by a lock-in amplifier were simulated based on the theory and formulations in our previous work [4]. The important simulation parameters mainly include the measured ICL tuning characters, the waveguide parameters, and the CO_2 absorption line profile obtained from the high-resolution transmission (HITRAN) database [13]. The measured relationship between the emitting wavenumber (WN, in cm^{-1}), the output power (P, in mW), and the current (I, in mA) of the ICL at an operation temperature of 0°C is $\mathrm{WN} = -0.087I + 2319.48$ and $P = 0.088I - 2.41$, respectively. The response coefficients (i.e., the slope of the response curve) of frequency (d Amp(D_{2f})/df_{sin} at 5 kHz) and intensity (d Amp(D_{2f})/dAmp_{sin} at 1.02 mA) to the sinusoidal modulation signal are numerically as small as -7.9×10^{-4} V/Hz and -2.0×10^{-5} V/mA, respectively, indicating that Amp(D_{2f}) nearly reaches the maximum at 5 kHz and 1.02 mA. As can be seen from Fig. 4(a), the simulation results of Amp(D_{2f}) are consistent with those from the experiment within 0%–100%.

The noise level of the sensor was evaluated to obtain the LoD using WMS. The measured 2f signals for 40% CO_2 ($C_{cell} = 40\%$) and N_2 ($C_{cell} = 0\%$) and the D_{2f} signal are shown in Fig. 4(b). The measured Amp(D_{2f}) was 2.83 mV, and the 1σ noise of the D_{2f} signal was determined to be $n_{1\sigma} = 0.06$ mV through long-term measurement. Then the LoD can be determined by [4]

$$\mathrm{LoD} = C_{cell}/\mathrm{SNR}_C = C_{cell}/(\mathrm{Amp}(D_{2f})/n_{1\sigma}). \quad (5)$$

Here, SNR_C is the signal-to-noise ratio under the concentration level of C_{cell}. The LoD can be calculated as ~ 0.8%.

Pure N_2 was injected into the gas cell to remove the CO_2 adsorbed by PDMS. Then a 10% CO_2 sample was injected for 34 s. The dynamic response curve is shown in Fig. 4(c). A peak can be observed during the injection. After that, the CO_2 concentration returned to the initial concentration level after the injection of N_2 at the end. Setting C_{cell} to be 10%, the curve of C_{space} versus measurement time is shown in Fig. 4(c). When the target CO_2 concentration in the gas cell was relatively stable, the measured averaged value of C_{space} is 0.04% with a variation of $\Delta C_{space} = 0.037\%$.

An Allan deviation analysis [Fig. 4(d)] was performed by the measurement of the Amp(D_{2f}) at the N_2 environment ($C_{cell} = 0\%$) for ~ 15 min, which also indicates the dominated noise type and level of the waveguide sensor system. The Allan deviation result shows a 1σ LoD of 0.3% for a 0.2 s averaging time, which is in the same order of magnitude as the LoD calculated based on Eq. (5). So the dynamic range of the sensor can be regarded to be 0.3%–100%. The noise mainly comes from environmental vibration, mode interference of the waveguide and fiber, the error of the gas mixing system (Environics 4000), and the temperature drift of the detector. The environmental vibration, which severely affects the coupling between the fiber and the waveguide, leads to a small optimum averaging time (0.8 s). The atmospheric CO_2 absorption can be treated as background absorption, which was subtracted from the absorption signal. So the atmospheric CO_2 doesn't affect the LoD calculation and Allan deviation analysis results. However, a measurement of the background signal is needed when the sensor is exposed to air.

For comparison, the DAS technique was used to evaluate the sensor performance, where a scan signal with a current range of 41–58 mA was used to drive the laser, generating a wavelength range of 4317.80–4321.10 nm. Under the atmospheric CO_2 concentration level ($C_{cell} = C_{space}$), the averaged absorption signals obtained from the waveguide with $L_{s,WG1} = 1$ cm and another waveguide with $L_{s,WG2} = 2$ cm on the same substrate were recorded [Fig. 5(a)] for the calculation of α_{int}. The two baselines were achieved to remove the gas absorption. As shown in Fig. 5(a), according to the amplitude of the fitting baselines $v_0(L_{s,WG})$ at 4319.3 nm, it can be estimated that $\alpha_{int}|_{dB/cm} = -10\log_{10}[v_0(L_{s,WG2})/v_0(L_{s,WG1})]/(L_{s,WG2} - L_{s,WG1}) = 5.1$ dB/cm. The absorption in Fig. 5(a) includes two parts: the first part is the free-space absorption, and the second part is the absorption from the sensing waveguide. Compared with the first part, the second part can be ignored because of an extremely small $L_{s,WG}$ and γ. The larger loss of the 2-cm-long waveguide made the output sensing signal smaller than that of the 1-cm-long sensing waveguide. That is why the two absorptions have different baselines. Under the condition of the same absorbance of free-space CO_2 the signal attenuations under the two cases were different.

Table 1. Comparison between the MIR ChG-on-MgF_2 Waveguide Sensor and Other MIR Waveguide Sensors

Refs.	Platform	λ (μm)	Gas	α_{int} (dB/cm)	γ (exp.)	L (cm)	L_{eff} (cm)	LoD	L_{eff} × LoD (cm)	Technique
[6]	SOI	4.24	CO_2	3	44%	0.32	0.1408	0.1%	0.01408%	DAS
[5]	Si-on-Si_3N_4	4.23	CO_2	—	19.5%	1	0.195	0.5%	0.0975%	DAS
[12]	ChG-on-SiO_2	3.31	CH_4	7	—	1	—	2.5%	—	DAS
This work	ChG-on-MgF_2	4.319	CO_2	5.1	4.6%	1	0.046	2.5%	0.115%	DAS
								0.3%	0.0138%	WMS

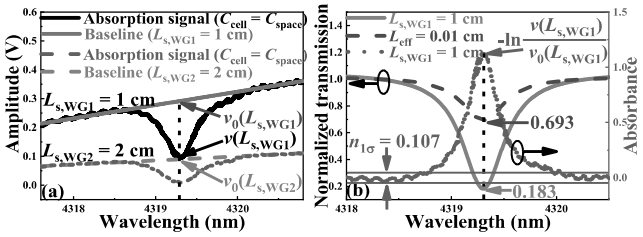

Fig. 5. (a) Averaged absorption signals from the waveguide with a length of 1 cm (black) and 2 cm (blue) with air in the gas cell and the baselines (red and green). (b) The fitting line of the normalized transmission curve of the waveguide (green, $C_{cell} = 40\%$, $L_{s,WG1} = 1$ cm), the simulated normalized transmission curve of free-space absorption (red, $C = C_{cell} = 40\%$, $L_{eff} = 0.01$ cm), and the absorbance signal (blue, $C_{cell} = C_{space}$, $L_{s,WG1} = 1$ cm) obtained from Fig. 5(a).

The normalized transmission of the sensing waveguide with $L_{s,WG1} = 1$ cm as well as the transmission with free-space absorption with an effective optical path length of L_{eff} is used to determine γ. The normalized transmission curve for the sensing waveguide ($L_{s,WG1} = 1$ cm, $C_{cell} = 40\%$) is shown in Fig. 5(b), which was obtained by a ratio operation between the absorption signal ($C_{cell} = 40\%$) and the background signal ($C_{cell} = 0\%$) with Lorentz fitting. Also, the simulated curve of free-space CO_2 absorption ($L_{eff} = 0.01$ cm, $C = C_{cell} = 40\%$) based on the HITRAN database [13] is shown in Fig. 5(b). The normalized transmission at the central wavelength for the waveguide is $\exp(-\gamma\alpha_{gas}C_{cell}L_{s,WG1}) = 0.183$, and the normalized value of the simulated free-space CO_2 absorption is $\exp(-\alpha_{gas}C_{cell}L_{eff}) = 0.693$. Therefore, γ can be estimated to be 4.6%.

Without modulation, the DAS-based sensor suffers from the influence of low-frequency noise. The absorbance signal [−ln(absorption signal/baseline)] obtained from Fig. 5(a) is shown in Fig. 5(b), whose 1σ noise is 0.107. Based on Eq. (5), the LoD can be calculated as $40\%/[-\ln(0.183)/0.107] = 2.5\%$.

A comparison between the proposed sensor and other gas sensors is shown in Table 1. The waveguide loss is smaller than the other ChG-on-SiO_2 sensors. The α_{gas} at 4.319 μm is at least 3 times lower than that in the ∼4.23 μm [5,6]. The LoD of this sensor based on DAS is higher than other waveguide CO_2 sensors because of the small L_{eff} ($L_{eff} = \gamma \times L_{s,WG}$) and α_{gas}. L_{eff} can be increased by reducing the waveguide width to increase γ or by increasing $L_{s,WG}$. L_{eff} × LoD represents the minimum detectable absorbance. Considering the difference in absorption line strength, the L_{eff} × LoD of the proposed sensor ($0.115\%/3 = 0.0383\%$) based on DAS is of the same order of magnitude as other CO_2 sensors (0.0141%, 0.0975%). Compared to DAS, the LoD of our sensor obtained by WMS can be decreased by >8 times. The proposed waveguide with a simple fabrication process and a small L_{eff} based on WMS can obtain the similar performance as other waveguides with better performances based on DAS. Therefore, under the same LoD requirement, the use of WMS technique is beneficial to the miniaturization of the sensor.

In conclusion, we proposed a novel ChG-on-MgF_2 waveguide gas sensor based on the WMS technique for the first time as far as we know. MgF_2 was used as the lower cladding layer to decrease the light power confined in the lower cladding layer. The simulation results showed that the γ can be increased by >40 times by using the MgF_2 as the lower cladding layer instead of the ChG glass with a refractive index of 2.2. The LoD of the waveguide gas sensor based on WMS was ∼0.3%, which was >8 times lower than that of the DAS. Using the WMS technique and a MgF_2 lower cladding layer, the performance of the sensor can be effectively improved, which is of great significance to the miniaturization of the waveguide sensor chip.

Funding. National Natural Science Foundation of China (61775079, 62175087, 61960206004, 61627823); Key Science and Technology RD program of Jilin Province, China (20200401059GX); Program for JLU Science and Technology Innovative Research Team (JLUSTIRT, 2021TD-39).

Disclosures. The authors declare no conflicts of interest.

Data Availability. The data that support the findings of this Letter are available from the corresponding author upon reasonable request.

REFERENCES

1. B. Schwarz, P. Reininger, D. Ristanić, H. Detz, A. M. Andrews, W. Schrenk, and G. Strasser, Nat. Commun. **5**, 4085 (2014).
2. Z. Liu, C. Zheng, T. Zhang, Y. Li, Q. Ren, C. Chen, W. Ye, Y. Zhang, Y. Wang, and F. K. Tittel, Anal. Chem. **92**, 8178 (2020).
3. K. Zheng, C. Zheng, J. Li, N. Ma, Z. Liu, Y. Zhang, Y. Wang, and F. K. Tittel, Sens. Actuators B **308**, 127674 (2020).
4. C. Li, C. Zheng, L. Dong, W. Ye, F. K. Tittel, and Y. Wang, Appl. Phys. B **122**, 185 (2016).
5. C. Ranacher, C. Consani, A. Tortschanoff, R. Jannesari, M. Bergmeister, T. Grille, and B. Jakoby, Sens. Actuators A **277**, 117 (2018).
6. F. Ottonello-Briano, C. Errando-Herranz, H. Rödjegård, H. Martin, H. Sohlström, and K. B. Gylfason, Opt. Lett. **45**, 109 (2020).
7. M. J. Dodge, Appl. Opt. **23**, 1980 (1984).
8. J. T. Robinson, K. Preston, O. Painter, and M. Lipson, Opt. Express **16**, 16659 (2008).
9. M. Vlk, A. Datta, S. Alberti, H. D. Yallew, V. Mittal, G. S. Murugan, and J. Jágerská, Light Sci. Appl. **10**, 26 (2021).
10. R. Siebert and J. Müller, Sens. Actuators A **119**, 138 (2005).
11. M. Pi, C. Zheng, J. Ji, H. Zhao, Z. Peng, J. Lang, L. Liang, Y. Zhang, Y. Wang, and F. K. Tittel, ACS Appl. Mater. Interfaces **13**, 32555 (2021).
12. Z. Han, P. Lin, V. Singh, L. Kimerling, J. Hu, K. Richardson, A. Agarwal, and D. T. H. Tan, Appl. Phys. Lett. **108**, 141106 (2016).
13. HITRAN online, The HITRAN Database, https://hitran.org/.